J Periodontal Implant Sci. 2020 Dec;50(6):392-405
https://doi.org/10.5051/jpis.1905680284
pISSN 2093-2278·eISSN 2093-2286

JPIS
Journal of Periodontal & Implant Science

Research Article
Implant Science

Check for updates

Chitosan/hydroxyapatite composite coatings on porous Ti6Al4V titanium implants: *in vitro* and *in vivo* studies

Ting Zhang [1,2], **Xinwei Zhang** [3], **Mengyun Mao** [4], **Jiayi Li** [5], **Ting Wei** [4], **Huiqiang Sun** [1,2,*]

[1]Shandong Provincial Key Laboratory of Oral Tissue Regeneration, Shandong University School of Stomatology, Jinan, China
[2]Department of Prosthodontics, Shandong University School of Stomatology, Jinan, China
[3]The Second Hospital of Anhui Medical University, Hefei, China
[4]Affiliated Stomatology Hospital, Zhejiang University School of Medicine, Hangzhou, China
[5]Department of Oral and Maxillofacial-Head Neck Oncology, Ninth People's Hospital, Shanghai Jiaotong University School of Medicine, Shanghai, China

OPEN ACCESS

Received: Nov 19, 2019
Revised: Mar 9, 2020
Accepted: Jun 5, 2020

***Correspondence:**
Huiqiang Sun
Shandong Provincial Key Laboratory of Oral Tissue Regeneration, Shandong University School of Stomatology, 44-1 Wenhuaxilu, Jinan 250010, China.
E-mail: whitedove69@163.com
Tel: +86-0531-88382058

ORCID iDs
Ting Zhang
https://orcid.org/0000-0001-6513-9917
Xinwei Zhang
https://orcid.org/0000-0002-7401-5243
Mengyun Mao
https://orcid.org/0000-0002-1858-9074
Jiayi Li
https://orcid.org/0000-0003-3515-9073
Ting Wei
https://orcid.org/0000-0001-6157-0056
Huiqiang Sun
https://orcid.org/0000-0002-8878-4676

Funding
This work was supported by the Key Research and Development Program of Shandong Province (2019GSF107001).

ABSTRACT

Purpose: Titanium implants are widely used in the treatment of dentition defects; however, due to problems such as osseointegration failure, peri-implant bone resorption, and peri-implant inflammation, their application is subject to certain restrictions. The surface modification of titanium implants can improve the implant success rate and meet the needs of clinical applications. The goal of this study was to evaluate the effect of the use of porous titanium with a chitosan/hydroxyapatite coating on osseointegration.
Methods: Titanium implants with a dense core and a porous outer structure were prepared using a computer-aided design model and selective laser sintering technology, with a fabricated chitosan/hydroxyapatite composite coating on their surfaces. *In vivo* and *in vitro* experiments were used to assess osteogenesis.
Results: The quasi-elastic gradient and compressive strength of porous titanium implants were observed to decrease as the porosity increased. The *in vitro* experiments demonstrated that, the porous titanium implants had no biological toxicity; additionally, the porous structure was shown to be superior to dense titanium with regard to facilitating the adhesion and proliferation of osteoblast-like MC3T3-E1 cells. The *in vivo* experimental results also showed that the porous structure was beneficial, as bone tissue could grow into the pores, thereby exhibiting good osseointegration.
Conclusions: Porous titanium with a chitosan/hydroxyapatite coating promoted MC3T3-E1 cell proliferation and differentiation, and also improved osseointegration *in vitro*. This study has meaningful implications for research into ways of improving the surface structures of implants and promoting implant osseointegration.

Keywords: Osseointegration; Dental implants; Titanium; Biocompatible materials; Porosity

INTRODUCTION

Titanium and titanium alloys are the preferred materials for oral implantation and bone replacement due to their good biocompatibility and corrosion resistance. However, the elastic

Author Contributions

Conceptualization: Huiqiang Sun, Xinwei Zhang; Formal analysis: Xinwei Zhang, Mengyun Mao; Investigation: Xinwei Zhang, Mengyun Mao; Methodology: Xinwei Zhang, Mengyun Mao; Project administration: Huiqiang Sun; Writing - original draft: Xinwei Zhang, Mengyun Mao; Writing - review & editing: Ting Zhang, Jiayi Li, Ting Wei, Huiqiang Sun.

Conflict of Interest

No potential conflict of interest relevant to this article was reported.

moduli differ considerably between titanium implants and the surrounding bone tissue. The elastic modulus for titanium implants is 103–110 GPa, while the elastic moduli for cortical bone and cancellous bone are 12.6–21 GPa and 0.5–3.5 GPa, respectively [1]. Thus, a portion of the stress transmitted to bone tissue is shared with the titanium implant due to its higher elastic modulus. This induces, bone resorption due to insufficient stimulation of stress on bone tissue and may cause alveolar bone remodeling, leading to the loosening or loss of the implant [2,3]. Recently, 2 strategies have been recommended to avert bone absorption via reduction of the elastic modulus: adding alloy elements, such as niobium, zirconium, and tin [4,5]; and building an osteoid porous structure within the titanium implant [6,7].

Porous titanium materials can simulate the loose and porous structure of bone tissue. El-Hajje et al. [8] found that the elastic modulus of titanium with a porosity of 32.2%–53.4% was 0.86–2.48 GPa, which fell within the range of the elastic modulus of cancellous bone. A gradient-porous titanium pillar prepared by Torres et al. [9,10] efficiently reduced the elastic modulus of the titanium pillar to match that of cortical bone. Porous titanium can promote the proliferation, differentiation, and mineralization of mesenchymal stem cells and osteoblasts [11,12]. However, excessive porosity can significantly reduce the compressive strength of the implant. The majority of studies have attempted to improve porous titanium implants by adding a central solid pillar or adopting a gradient-porous design to avoid implant deformation or fracture [13,14]. Consequently, a structure with a dense core and a porous outer layer can further improve porous titanium implants and reduce their elastic moduli, while ensuring their compressive strength. However, a porous titanium implant cannot be prepared using traditional casting technology due to its sophisticated structure and controlled porosity.

The development of digitization and automation has promoted the widespread use of 3-dimensional (3D) printing technology in biomedicine, with techniques including selective laser sintering (SLS) and fused deposition modeling. SLS technology utilizes computer-aided design modeling [15-17]. Powder particles are selectively sintered with laser beams and overlaid layer by layer, ultimately forming a 3D model [18,19]. In this fashion, SLS technology can produce items with sophisticated structures and highly accurate sizes. Moreover, SLS can reduce material consumption and avoid chemical contamination.

A prerequisite for successful dental implantation is osseointegration, for which the properties of the materials used are crucial. However, titanium is a bioinert material. Surface modification, such as the preparation of a biocoating, is imperative to improve osseointegration. However, desquamation of the biocoating on solid implants may occur during implantation, and is detrimental to osseointegration and biosecurity. Nevertheless, a biocoating on the porous structure can remain intact in the inner walls of the holes and accelerate new bone formation. Hydroxyapatite (HA) is an inorganic constituent in bone, and it has excellent biocompatibility and bone inductivity. However, HA easily becomes detached from materials due to its low intensity and high brittleness. Chitosan (CS), a natural alkaline polysaccharide, is biodegradable and is not cytotoxic. The combination of HA and CS exhibits favorable hardness, and a CS/HA composite coating has high biocompatibility. The rough microtopography of this coating increases the contact area of the implant-bone interface and has been shown to demonstrate good bone inductivity [20].

Osteoblast-like MC3T3-E1 cells are derived from the mouse cranium, and have been widely used as a model for bone biology research [21,22]. As described in our previous work,

https://doi.org/10.5051/jpis.1905680284

Table 1. Ti6Al4V specimens used in the static state test of mechanical properties

Cylindrical Ti6Al4V specimen with a dense core and a porous outer layer (diameter, 8 mm; height, 15 mm; solid pillar diameter, 4 mm)	Cylindrical Ti6Al4V test specimen with a completely porous layer (diameter, 8 mm; height, 15 mm)
30% porosity	30% porosity
45% porosity	45% porosity
60% porosity	60% porosity

osteoblast-like MC3T3-E1 cells exhibit good proliferation and differentiation on titanium slices [23]. In the present study, we used SLS technology to prepare titanium implants of various porosities both with and without a dense core [24]. In addition, we fabricated a CS/HA composite coating on the surface of the porous titanium [14,20]. The biocompatibility of CS/HA-incorporated porous titanium implants was evaluated according to the proliferation of MC3T3-E1 cells. Furthermore, an *in vivo* rabbit experiment was performed to evaluate the osseointegration of the porous titanium implants.

MATERIALS AND METHODS

Design and fabrication of porous titanium

A 3D model of porous titanium was designed with the Rhino 3D modeling software (Robert McNeel & Associates, Seattle, WA, USA). The inner pores (diameter, 400 μm) were interconnected. The pillar diameter of the porous structure was at least 300 μm, and the porosity was adjusted according to the experimental design. The cylindrical Ti6Al4V specimens used in the static-state test of mechanical properties are listed in Table 1. Group I specimens had a dense core and a porous outer layer, while group II specimens had a completely porous structure. The Ti6Al4V disks and Ti6Al4V thread implants used in the *in vitro* and *in vivo* experiments are described in Tables 2 and 3, respectively. The surface of each thread implant was engraved with a T-shaped thread, and 3D-porous titanium was produced with an SLS device. Then, the test specimens were soaked in an acid mixture composed of 49% H_2SO_4 and 19% HCl (1:1) for acid etching with subsequent ultrasonic cleaning with the Micro 90® concentrated alkaline cleaning solution (International Products Corporation, Burlington, NJ, USA) using a sequence of cleaning solution, absolute ethyl alcohol, and deionized water. A total of 1.98 grams of $Ca(NO_3)_2{\cdot}4H_2O$ and 0.66 grams of KH_2PO_4 were dissolved in distilled water, and 1 gram of chitosan powder was dissolved in 100 mL of 2% acetic acid. The 2 solutions were mixed to prepare a CS/HA composite coating on the surface of the porous titanium using an electrochemical deposition method [24].

Table 2. Ti6Al4V specimens used in in vitro experiments

Group	Ti6Al4V disk (diameter, 20 mm; thickness, 2 mm)
A	0% porosity (completely solid)
B	30% porosity (solid lower layer thickness, 1 mm; porous upper layer thickness, 1 mm)
C	50% porosity (solid lower layer thickness, 1 mm; porous upper layer thickness, 1 mm)

Table 3. Ti6Al4V specimens used in in vivo experiments

Group	Ti6Al4V implant (diameter, 3.5 mm; height, 7 mm; solid pillar diameter, 1.5 mm)
A	0% porosity (completely solid)
B	30% porosity (solid pillar diameter, 1 mm; porous outer layer thickness, 1 mm)
C	40% porosity (solid pillar diameter, 1 mm; porous outer layer thickness, 1 mm)
D	50% porosity (solid pillar diameter, 1 mm; porous outer layer thickness, 1 mm)

https://doi.org/10.5051/jpis.1905680284

Surface morphology and mechanical properties of porous titanium

A scanning electron microscope (SEM) (JSM-6610LV; JEOL, Tokyo, Japan) was used to observe the surface characteristics of the test specimens, which included the solid implants and the implants with dense cores and porous outer layers. A compression test was performed using a universal material machine. The results were graphed as a stress-strain curve.

In vitro experiment

MC3T3-E1 cell culture and inoculation

Osteoblast-like MC3T3-E1 cells (Chinese Academy of Sciences Cell Bank, Shanghai, China) were cultured in α-modified Eagle medium (HyClone, Logan, UT, USA) containing 10% fetal bovine serum (Sijiqing, Hangzhou, China), 1% 100 U/mL penicillin, and 100 g/mL streptomycin (Solarbio Life Sciences, Beijing, China) in a constant temperature and humidity incubator at 37°C and 5% CO_2. MC3T3-E1 cells were inoculated on the surfaces of the titanium disks at a density of 5×10^4 cells per disk. The cells on the titanium disks were incubated at 37°C in a fully humidified atmosphere of 5% CO_2 in air, and the medium was changed every 2 days.

Living/dead cell vitality assay

After 1, 3, and 7 days of incubation on the titanium disks, cell vitality was determined with a live/dead cell staining kit (Shanghai Hengfei Biotechnology Co., Ltd., Shanghai, China). At least 6 images in different views were produced for each disk. The images were analyzed with Image-Pro Plus 6.0 software (Media Cybernetics, Inc., Rockville, MD, USA).

Alkaline phosphatase (ALP) activity assay

Cell differentiation on the titanium disks after 7 days was detected using an ALP activity assay. The cells were lysed with 1% Triton-X 100. Then, protein concentrations were measured with a bicinchoninic acid protein assay kit (Wuhan Boster Biological Technology, Ltd., Wuhan, China). The absorbance values were measured at 520 nm with a microplate reader, and ALP activity was calculated according to the absorbance values.

In vivo animal experiment

Animal experiment

The animal experiment was approved by the Animal Ethics Committee of Shandong University, and the experimental protocol adhered to Shandong University's Guidelines for the Care and Use of Laboratory Animals. Six male white New Zealand rabbits were selected (2.7–3.2 kg, age 14–16 weeks; source, Jinan Xilingjiao Cultivation and Breeding Center) and fed a standard diet for 7 days. After preoperative fasting for 12 hours, general anesthesia with chloral hydrate (Cheeloo Hospital, Jinan, Shandong, China) (1–1.2 mL/kg) combined with local anesthesia with lidocaine was administered. A 2.5 cm longitudinal incision was made in the proximal area of the femoral condyle. Two defects with diameters of 3.5 mm and depths of 7 mm were drilled in each lower limb. Two implants with different porosities were randomly inserted into the defects, and each wound was closed with a conventional suture. Cefazolin sodium (Shandong Lukang Pharmaceutical Co., Ltd., Shandong, China) was injected in the case of infection. After surgery, the rabbits were carefully observed and fed a standard diet. All operations were performed by the same skilled surgeon with 2 assistants, and the individual who inserted the implants was blinded to the implant design.

Histological analysis

The rabbits were sacrificed on weeks 4 and 12 after the operation. The samples (each consisting of the implant and the surrounding 1 cm of bone tissue) were harvested at the

https://doi.org/10.5051/jpis.1905680284

bilateral femoral condyles, and the soft tissue was removed. After the samples were rinsed with saline, an X-ray examination was performed to observe the implantation. The samples were then immediately soaked in 4% paraformaldehyde solution (Wuhan Servicebio Technology Co., Ltd., Wuhan, China) for 24 hours. After rinsing under running water for 4 to 6 hours, the samples were dehydrated stepwise in 50%–100% alcohol for 48 hours. Then, they were placed in an E510 infiltrator and soaked in plastic dipping solutions 1, 2, 3, and 4 for 48 hours each to yield polymethacrylic resin-embedded samples. A hard tissue slicing machine (EXAKT, Norderstedt, Germany) was used to produce 30-μm-thick hard tissue slices along the long axis of the implant. Then, the slices were stained with methylene blue/acid fuchsin (Shanghai Enzyme-linked Biotechnology Co., Ltd., Shanghai, China) after ultrasonic cleaning for 5 minutes in triple-distilled water. Osseointegration of the implants was detected with an optical microscope (OLYMPUS, Tokyo, Japan).

Statistical methods

Statistical software (SPSS version 24.0; IBM Corp., Armonk, NY, USA) was used to analyze the experimental results. The *t*-test was used for continuous variables, and *P* values ≤0.05 were considered to indicate statistical significance.

RESULTS

Preparation of porous implants

The 3D models (in STL file format) depicted the porous-thread implants from all angles (Figure 1A). The surfaces of the cylindrical titanium specimens did not display any redundant powder (Figure 1B). The inner pores were interconnected, and the surfaces of the titanium disks (Figure 1C) appeared to exhibit some microroughness. The pores were well-distributed and of consistent size. The T-shaped thread on the surface of each thread implant specimen (Figure 1D) was continuous and smooth. The pore structure was interlaced in multiple directions, and the pore sizes near the thread were unevenly distributed.

Surface topography of specimens

Figure 2A-D shows the SEM images of the titanium specimens that were untreated (that is, that lacked surface modification). Under low magnification, the solid implant (Figure 2A) appeared to exhibit microtopography without obvious casting defects, and the porous implant with a dense core (Figure 2B and C) also exhibited microroughness. The pitch of the trapezoidal thread was approximately 1 mm, and its depth was 0.3 mm. The pores were observed to be evenly distributed and to exhibit inner connectivity. The observed pore size was approximately 400 μm. Several partially melted titanium powder particles adhered to the inner wall, and the diameters of these particles were approximately 25 μm as seen under high magnification (Figure 2D). Figures 2E and 2F show the SEM images of the CS/HA coatings deposited using an electrochemical treatment. Under high magnification, the coating appears as an even, dense lamellar structure, with few cracks and micropores on the surface.

Quasi-elastic gradient and compressive strength of specimens

As shown in Figure 3A, the specimens with 30% porosity had the highest quasi-elastic gradient, while the specimens with 60% porosity had the lowest gradient. When the porosity of the specimens was the same, the quasi-elastic gradient in group II was slightly lower than that in group I. The compressive strength was consistent with the quasi-elastic gradient and differed significantly between groups (Figure 3B). Additionally, in group I, the elastic

https://doi.org/10.5051/jpis.1905680284

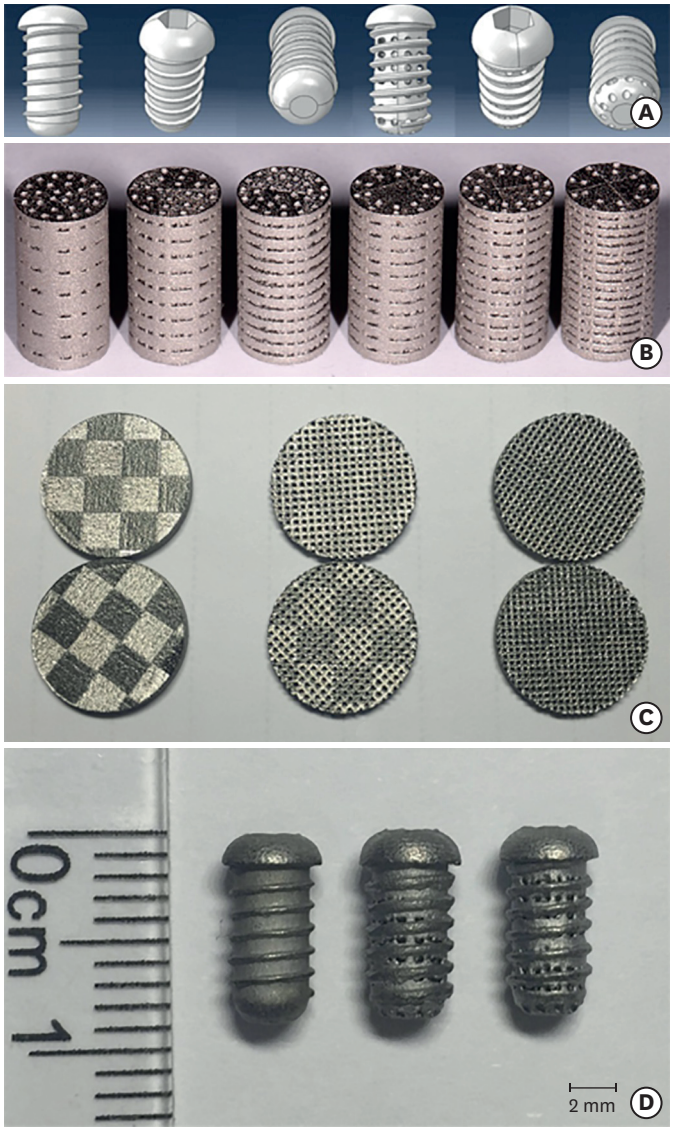

Figure 1. 3D models of porous titanium thread implants and the Ti6Al4V test specimens prepared with selective laser sintering technology. (A) The 3D models of the porous-thread implant. (B) Cylindrical titanium alloy test specimens. (C) Discoid titanium alloy test specimens. (D) Thread implant test specimens.
3D: three-dimensional.

modulus for the specimen with 30% porosity was 34.3 GPa, while that for the sample with 60% porosity was 4.63 GPa; these values are close to the moduli of human cortical bone and cancellous bone, respectively.

Living/dead cell vitality assay

Cells on the surfaces of the titanium disks with porosities of 0%, 30%, and 50% appeared highly active on day 1, day 3, and day 7. The fraction of live cells was greater than 85%, and no significant differences were observed between the 3 groups. On day 1 (Figure 4A-C), most of the osteoblasts were seen to adhere to the surface of the solid titanium and the pillar of the porous titanium, and few cells adhered to the inner walls of the pores. On day 3 (Figure 4D-F), the cells in the pores of the porous titanium plate were observed to have rapidly

https://doi.org/10.5051/jpis.1905680284

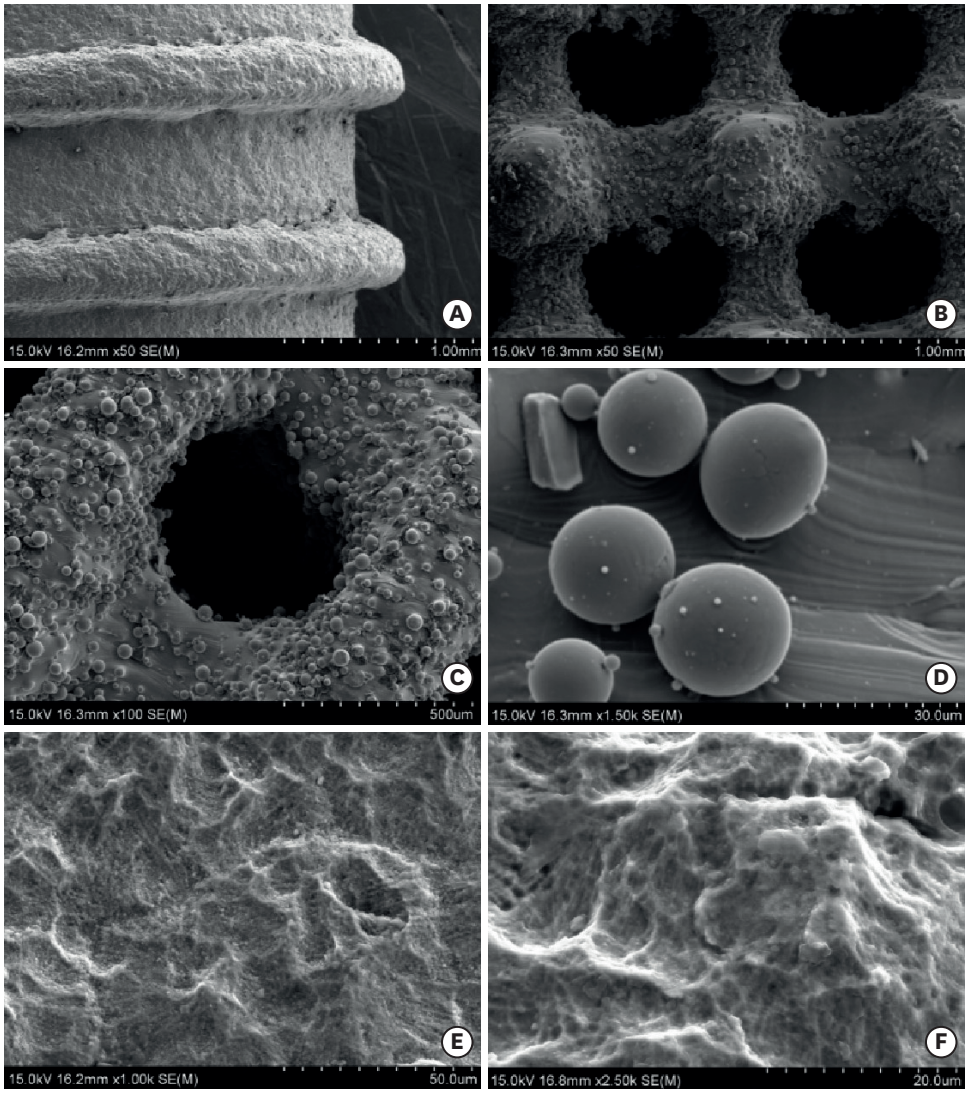

Figure 2. Scanning electron microscopy images of the titanium alloy test specimens. (A) Surface appearance of the solid-thread implant under low magnification (×50). (B) Appearance of the pores in the porous titanium test specimen under low magnification (×50). (C) Appearance of the pores in the porous titanium test specimen under low magnification (×100). (D) The titanium powder particles were not completely melted, as shown under high magnification (×1,500). (E) Chitosan/hydroxyapatite coatings prepared through an electrochemical deposition method at ×1,000 and (F) ×2,500 magnification.

proliferated and adhered to the inner walls, where they began to contact each other. On day 7 (Figure 4G-I), the density of the cells on the solid titanium was observed to have increased by 90% or more. Meanwhile, the cells on the pillar of the porous titanium had grown to a high density, displaying contact inhibition. Imaging under high magnification revealed that cells adhered to the uneven surfaces of the pores of the porous titanium (Figure 4J).

ALP activity assay

As shown in Figure 5, the ALP activity on the titanium with the CS/HA coating was higher than the activity on the titanium with no CS/HA coating (P<0.05). In addition, the ALP activity of the porous titanium was higher than that of the solid titanium (P<0.05).

https://doi.org/10.5051/jpis.1905680284

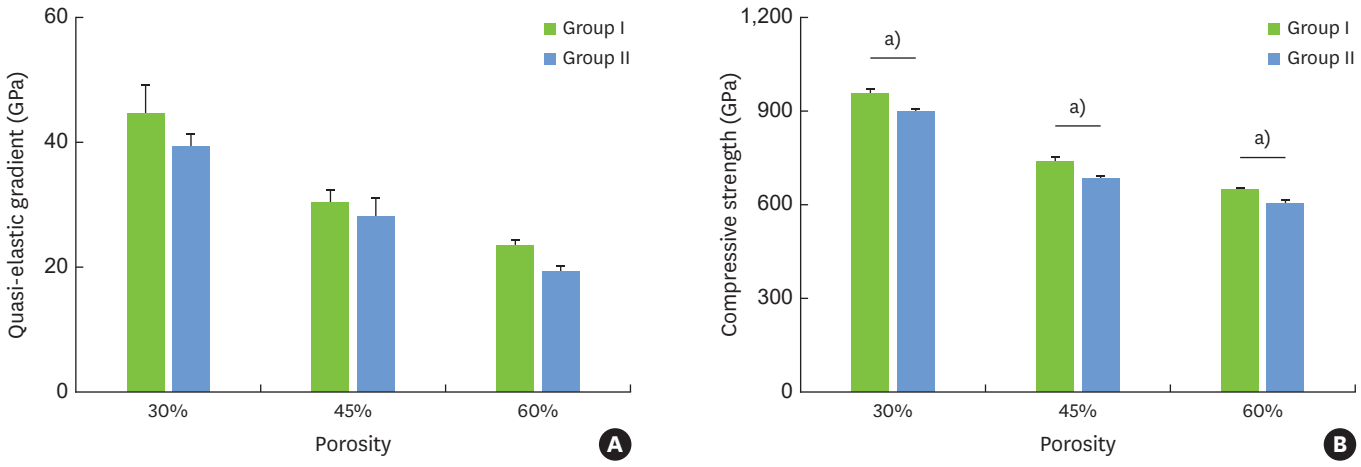

Figure 3. (A) Quasi-elastic gradient and (B) compressive strength of the titanium specimens with a dense core and porous outer layer (group I) and with a completely porous structure (group II). The error bars correspond to the standard deviation.
[a)]Corresponds to significant differences in the compressive strength between group I and group II at the same porosity.

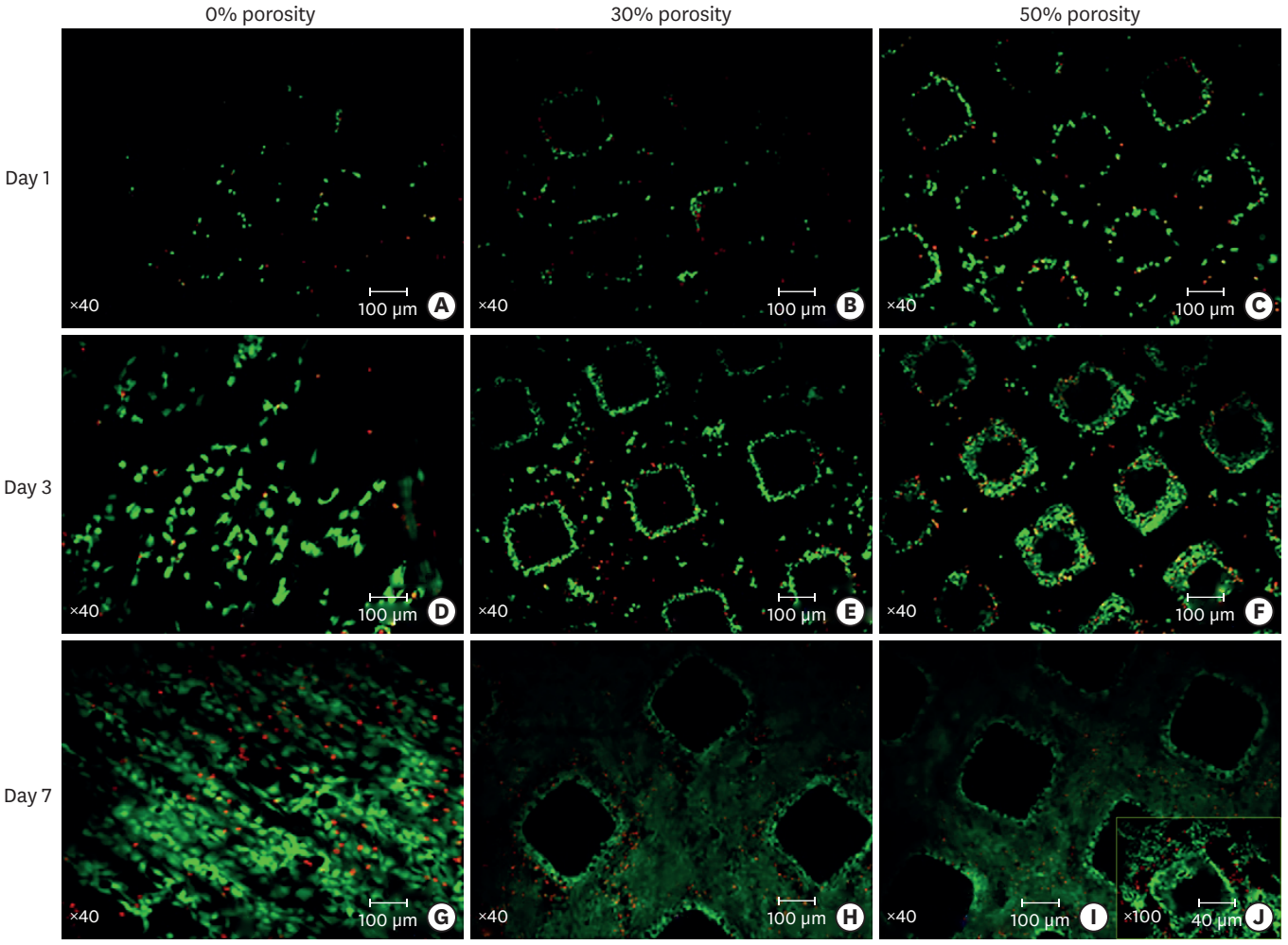

Figure 4. Staining of live/dead cells on the titanium plates with porosities of 0%, 30%, and 50%. Live cells are green, while dead cells are red due to the adhesion of propidium iodide. (A-C) Day 1 (×40). (D-F) Day 3 (×40). (G-I) Day 7 (×40). (J) Image taken under high magnification (×100). Ratio of live cells=number of live cells/(number of live cells+number of dead cells in the same field of view).

https://doi.org/10.5051/jpis.1905680284

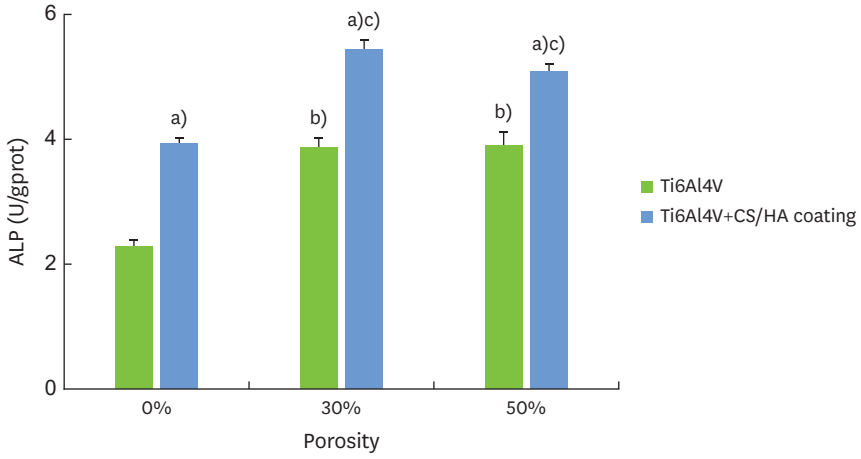

Figure 5. Alkaline phosphatase levels of the MC3T3-E1 cells on the surface of the titanium plates with different porosities and covered with the chitosan/hydroxyapatite coatings.
ALP: alkaline phosphatase, CS: chitosan, HA: hydroxyapatite.
[a]Corresponds to significant differences between Ti6Al4V and Ti6Al4V+CS/HA coating; [b]Corresponds to significant differences between this group and 0% Ti6Al4V; [c]Corresponds to significant differences between this group and 30% Ti6Al4V.

X-ray examination

Figure 6A shows the implantation at the bilateral femoral condyles. Samples were collected from animals sacrificed on weeks 4 and 12. An X-ray examination was performed to visualize the implantation (Figure 6B). The implant angle was normal, and the distance between the 2 implants was appropriate. Furthermore, the surrounding bone had healed well without any fractures or fissures.

Histological analysis

Figure 7 shows methylene blue- and magenta-stained images of hard tissue slices. After implantation for 4 weeks, contact osteogenesis was observed under low magnification (Figure 7A-C) on the surfaces of the implants, and new bone was observed to have been produced inside the pores of the porous implant. Examination under high magnification

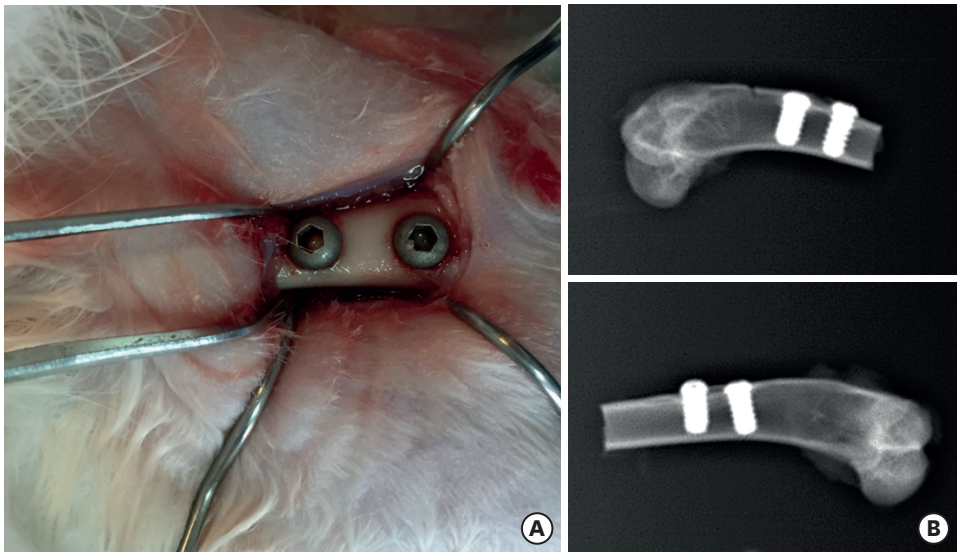

Figure 6. (A) Implantation at the bilateral femoral condyles. (B) X-ray examination.

https://doi.org/10.5051/jpis.1905680284

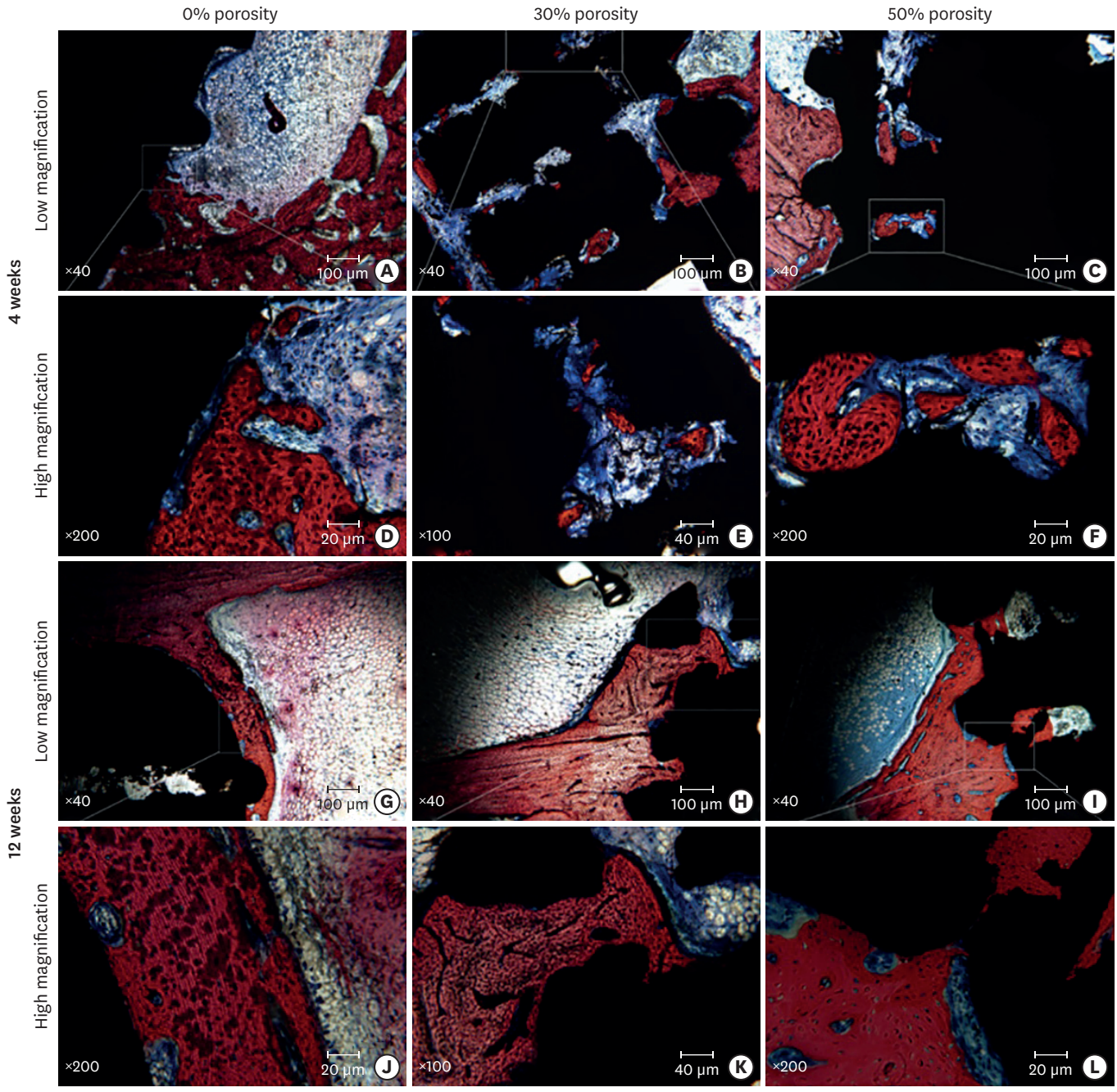

Figure 7. Methylene blue/acid fuchsin staining of the implants with porosities of 0%, 30%, and 50% implanted into the rabbit femoral condyle after (A-F) 4 weeks and (G-L) 12 weeks. The new bone tissue is dark red, the original mineralized tissue is red, the osteoblast nuclei are dark blue, the cell matrix is light blue, the osteoid is blue-violet, and the implant is black. (A-C) Images under low magnification at week 4. (D-F) Images under high magnification at week 4. (G-I) Images under low magnification at week 12. (J-L) Images under high magnification at week 12.

(Figure 7D-F) revealed that the osteoblasts around the implant were densely packed and that many active osteoblasts were present in the pores of the porous implant; moreover, the new trabecular bone appeared slender and relatively bright and was stained dark red. By week 12, the trabecular bone had become thicker than that at week 4, and the contact osteogenesis was more obvious. The number of new bone areas in the pores of the porous implant had increased compared to the discontinuous distribution observed at week 4, and

https://doi.org/10.5051/jpis.1905680284

the areas had a tendency to connect with each other (Figure 7G-I). An examination under high magnification (Figure 7J-L) revealed that large pores close to the surface were filled with new bone tissue; the trabecular bone was thick and dense with clusters of active osteoblasts surrounding the bone. No inflammatory cell infiltration was detected.

DISCUSSION

SLS technology is directly driven by the computer-aided design model, allowing the rapid production of a 3D model with high precision and complexity. SLS technology is beneficial for the preparation of porous structural implants, which can stimulate trabecular bone for optimal osseointegration.

Most artificial porous implants have a homogeneous structure with regard to pore size, unlike the pores of human trabecular bone [25]. Cheng et al. [15,26] prepared an imitation of trabecular porous structures with variable porosity based on computed tomography images of human femoral trabecular bone and found that the MG63 cells on the material were highly active and were able to grow into the pores. Pattanayak et al. [27] observed new bone formation in the inner pores of an imitation trabecular porous implant, and the new bone was found to attach in the vicinity of the pores. An imitation trabecular porous structure can stimulate osteoblast activity and induce osteogenesis. However, weak points of the imitation trabecular porous structure are unavoidable and may lead to implant deformation and fracture under masticatory force. In the present experiment, the porous implants had a lower quasi-elastic gradient than the solid implants, and the quasi-elastic gradient was observed to decrease as porosity increased. Furthermore, the quasi-elastic gradients of the implants with porosities of 30% and 70% were consistent with the gradients of human cortical bone and cancellous bone, respectively. The porous titanium implant prepared in this study has a dense central core and can be modulated with regard to pore size and porosity to achieve the required mechanical strength.

Osteoblasts have been demonstrated to exhibit sensitivity to surface topography. The hierarchy roughness of a porous structure plays a central role in the biological behavior of osteoblasts. Our *in vitro* experiments demonstrated that porous implants covered with a CS/HA coating had good biocompatibility, which promoted osteoblast proliferation and differentiation and also increased the surface area available for cell adhesion. Furthermore, the internally-connected pores provided nutrient and waste transport, accelerated cell metabolism, and promoted cell proliferation and differentiation.

Porous structures can facilitate osseointegration. Ding et al. [28] implanted porous titanium fabricated with SLS into the rabbit radial bone and found that the microporous scaffold exhibited excellent osseointegration and vascularization. Muñoz et al. [29] investigated the interaction between the porosity and the mechanical properties of titanium. The performance of titanium structures with porosities of 37% and 47% resembled those of cortical bone and cancellous bone, respectively. Our *in vivo* results demonstrated that porous titanium has good biocompatibility. The hard tissue slice results showed that porous implants mainly relied on osseointegration on the external surface and on new trabecular bone in the interconnected pores. Porous titanium promotes osteogenesis and leads to biological fixation, which subsequently improves the implantation success rate. However, the molecular mechanism of these effects requires further study. A limitation of this article

https://doi.org/10.5051/jpis.1905680284

is that the surface of the sample was not examined in more detail. To further explore the improved performance mechanism of this material, energy-dispersive X-ray spectroscopy, X-ray diffraction, and attenuated total reflection Fourier-transform infrared spectroscopy should be used to analyze the CS/HA composite coating in subsequent experiments.

In conclusion, our findings demonstrated that porous titanium with a dense core had appropriate mechanical characteristics for implantation. The results of our experiments showed that porous titanium with a CS/HA coating could promote the proliferation and differentiation of MC3T3-E1 cells and osseointegration *in vivo*. The findings of this study have important implications for the optimization of dental and orthopedic implants.

ACKNOWLEDGEMENTS

The titanium specimens were fabricated with the assistance of Shandong Maier Medical Technology Co., Ltd.

REFERENCES

1. Wu SL, Liu XM, Yeung KW, Guo H, Li P, Chu PK, et al. Surface nano-architectures and their effects on the mechanical properties and corrosion behavior of Ti-based orthopedic implants. Surf Coat Tech 2013;233:13-26.
CROSSREF
2. Traini T, Mangano C, Sammons RL, Mangano F, Macchi A, Piattelli A. Direct laser metal sintering as a new approach to fabrication of an isoelastic functionally graded material for manufacture of porous titanium dental implants. Dent Mater 2008;24:1525-33.
PUBMED | CROSSREF
3. Cook SD, Klawitter JJ, Weinstein AM. The influence of implant elastic modulus on the stress distribution around LTI carbon and aluminum oxide dental implants. J Biomed Mater Res 1981;15:879-87.
PUBMED | CROSSREF
4. Zhao D, Chang K, Ebel T, Qian M, Willumeit R, Yan M, et al. Microstructure and mechanical behavior of metal injection molded Ti-Nb binary alloys as biomedical material. J Mech Behav Biomed Mater 2013;28:171-82.
PUBMED | CROSSREF
5. Nie L, Zhan Y, Hu T, Chen X, Wang C. β-Type Zr-Nb-Ti biomedical materials with high plasticity and low modulus for hard tissue replacements. J Mech Behav Biomed Mater 2014;29:1-6.
PUBMED | CROSSREF
6. Jorgensen DJ, Dunand DC. Structure and mechanical properties of Ti-6Al-4V with a replicated network of elongated pores. Acta Mater 2011;59:640-50.
CROSSREF
7. Li F, Li J, Xu G, Liu G, Kou H, Zhou L. Fabrication, pore structure and compressive behavior of anisotropic porous titanium for human trabecular bone implant applications. J Mech Behav Biomed Mater 2015;46:104-14.
PUBMED | CROSSREF
8. El-Hajje A, Kolos EC, Wang JK, Maleksaeedi S, He Z, Wiria FE, et al. Physical and mechanical characterisation of 3D-printed porous titanium for biomedical applications. J Mater Sci Mater Med 2014;25:2471-80.
PUBMED | CROSSREF
9. Torres Y, Trueba P, Pavon J, Montealegre I, Rodriguez-Ortiz JA. Designing, processing and characterisation of titanium cylinders with graded porosity: An alternative to stress-shielding solutions. Mater Des 2014;63:316-24.
CROSSREF
10. Torres Y, Trueba P, Pavón JJ, Chicardi E, Kamm P, García-Moreno F, et al. Design, processing and characterization of titanium with radial graded porosity for bone implants. Mater Des 2016;110:179-87.
CROSSREF

11. Luthringer BJ, Ali F, Akaichi H, Feyerabend F, Ebel T, Willumeit R. Production, characterisation, and cytocompatibility of porous titanium-based particulate scaffolds. J Mater Sci Mater Med 2013;24:2337-58.
PUBMED | CROSSREF

12. Ninomiya JT, Struve JA, Krolikowski J, Hawkins M, Weihrauch D. Porous ongrowth surfaces alter osteoblast maturation and mineralization. J Biomed Mater Res A 2015;103:276-81.
PUBMED | CROSSREF

13. de Vasconcellos LM, Oliveira FN, Leite DO, de Vasconcellos LG, do Prado RF, Ramos CJ, et al. Novel production method of porous surface Ti samples for biomedical application. J Mater Sci Mater Med 2012;23:357-64.
PUBMED | CROSSREF

14. Wang GQ, Zver'kov DA, Zhang NS. Titanium based hydroxyapatite/chitosan coating prepared by microarc oxidation process and its biological characteristics. Rare Met Mater Eng 2013;42:2586-9.

15. Cheng A, Humayun A, Cohen DJ, Boyan BD, Schwartz Z. Additively manufactured 3D porous Ti-6Al-4V constructs mimic trabecular bone structure and regulate osteoblast proliferation, differentiation and local factor production in a porosity and surface roughness dependent manner. Biofabrication 2014;6:045007.
PUBMED | CROSSREF

16. Wieding J, Jonitz A, Bader R. The effect of structural design on mechanical properties and cellular response of additive manufactured titanium scaffolds. Materials (Basel) 2012;5:1336-47.
CROSSREF

17. Van der Stok J, Van der Jagt OP, Amin Yavari S, De Haas MF, Waarsing JH, Jahr H, et al. Selective laser melting-produced porous titanium scaffolds regenerate bone in critical size cortical bone defects. J Orthop Res 2013;31:792-9.
PUBMED | CROSSREF

18. Beaman JJ, Deckard CR. Selective laser sintering with assisted powder handling: US 1990.

19. Dillon PM, Chakraborty S, Moskaluk CA, Joshi PJ, Thomas CY. Adenoid cystic carcinoma: a review of recent advances, molecular targets, and clinical trials. Head Neck 2016;38:620-7.
PUBMED | CROSSREF

20. Kim BS, Kim JS, Chung YS, Sin YW, Ryu KH, Lee J, et al. Growth and osteogenic differentiation of alveolar human bone marrow-derived mesenchymal stem cells on chitosan/hydroxyapatite composite fabric. J Biomed Mater Res A 2013;101:1550-8.
PUBMED | CROSSREF

21. Xie B, Wu J, Li Y, Wu X, Zeng Z, Zhou C, et al. Geniposide alleviates glucocorticoid-induced inhibition of osteogenic differentiation in MC3T3-E1 cells by ERK pathway. Front Pharmacol 2019;10:411.
PUBMED | CROSSREF

22. Suzuki H, Tatei K, Ohshima N, Sato S, Izumi T. Regulation of MC3T3-E1 differentiation by actin cytoskeleton through lipid mediators reflecting the cell differentiation stage. Biochem Biophys Res Commun 2019;514:393-400.
PUBMED | CROSSREF

23. Wei T, Li J, Sun H, Jiang M, Yang Y, Luo X, et al. Verification of osteoblast differentiation on airborne-particle abrasion, large-grit, acid-etched surface of titanium implants regulated by yes-associated protein and transcriptional coactivator with PDZ-binding motif. J Oral Sci 2019;61:431-40.
PUBMED | CROSSREF

24. Pang X, Zhitomirsky I. Electrophoretic deposition of composite hydroxyapatite-chitosan coatings. Mater Charact 2007;58:339-48.
CROSSREF

25. Zaharin HA, Abdul Rani AM, Azam FI, Ginta TL, Sallih N, Ahmad A, et al. Effect of unit cell type and pore size on porosity and mechanical behavior of additively manufactured Ti6Al4V scaffolds. Materials (Basel) 2018;11:2402.
PUBMED | CROSSREF

26. Cheng A, Humayun A, Boyan BD, Schwartz Z. Enhanced osteoblast response to porosity and resolution of additively manufactured Ti-6Al-4V constructs with trabeculae-inspired porosity. 3D Print Addit Manuf 2016;3:10-21.
PUBMED | CROSSREF

27. Pattanayak DK, Fukuda A, Matsushita T, Takemoto M, Fujibayashi S, Sasaki K, et al. Bioactive Ti metal analogous to human cancellous bone: Fabrication by selective laser melting and chemical treatments. Acta Biomater 2011;7:1398-406.
PUBMED | CROSSREF

28. Ding R, Wu Z, Qiu G, Wu G, Wang H, Su X, et al. Selective Laser Sintering-produced porous titanium alloy scaffold for bone tissue engineering. Zhonghua Yi Xue Za Zhi 2014;94:1499-502.
PUBMED

29. Muñoz S, Pavon J, Rodriguez-Ortiz JA, Civantos A, Allain JP, Torres Y. On the influence of space holder in the development of porous titanium implants: mechanical, computational and biological evaluation. Mater Charact 2015;108:68-78.
CROSSREF